[3]E. W. Rothe, P. K. Rol, S. M. Trujillo, and R. H. Neynaber, Phys. Rev. 128, 659 (1962).
[4]E. A. Gislason and G. H. Kwei, J. Chem. Phys. 46, 2838 (1967).
[5]H. L. Kramer and P. R. LeBreton, J. Chem. Phys. 47, 3367 (1967).
[6]R. E. Olson and R. B. Bernstein, J. Chem. Phys. 49, 162 (1968).
[7]R. T. Cross, Jr., J. Chem. Phys. 49, 1976 (1968).
[8]D. A. Micha, Bull. Am. Phys. Soc. 13, 394 (1968); J. Chem. Phys. (to be published, 1969).
[9]R. Marriott, Proc. Phys. Soc. (London) 72, 121 (1958), Appendix.
[10]A. C. Allison and A. Dalgarno, Proc. Phys. Soc. (London) 90, 609 (1967), show the contribution of individual partial waves to rotational excitation cross sections.
[11]R. B. Bernstein, Advances in Chemical Physics, edited by J. Ross (Interscience Publishers, New York, 1966) Vol. X, Chap. 3.
[12]C. Nyland and J. Ross, J. Chem. Phys. 49, 843 (1968).
[13]R. B. Bernstein and R. D. Levine, J. Chem. Phys. 49, 3872 (1968).

PHYSICAL REVIEW VOLUME 180, NUMBER 1 5 APRIL 1969

Threshold Behavior of the Cross Section for Ionization of He and Ar by Mono-Energetic Electrons*

P. Marchand, C. Paquet, and P. Marmet
Centre de Recherches Sur Les Atomes et Les Molécules, Laval University, Quebec, Canada
(Received 26 August 1968; revised manuscript received 16 December 1968)

A new apparatus using crossed-beam techniques with a cylindrical electrostatic electron velocity selector for the study of ionization probability curves of gases is described. Results for He^+ and Ar^+ in the first eV above the ionization threshold are given. New computer techniques determine structure and near-threshold behavior. A simple power law yields a good representation of the experimental results for each ion state, with a different power in each case. For He a power law with power 1.16 is found. The results for Ar may be represented by two power laws with powers 1.3 and 1.34, respectively, joining at the energy of the $^2P_{1/2}$ level of Ar^+.

INTRODUCTION

The study of ionization by electron impact near the ionization threshold is of considerable interest for the determination of electron-neutral interaction laws, and has been the object of a considerable number of experimental and theoretical works. The experimental work, however, has not yet always yielded the results hoped for, as witnessed by the lack of agreement between the results from different laboratories and by the lack of reproducibility of results in general.

For instance, there has been considerable difficulty in the past in obtaining sufficiently large currents of fairly monoenergetic electrons at energies from 10 to 25 eV. Although the introduction of the retarding-potential-difference (RPD) method[1] and of spherical[2] and cylindrical[3] electrostatic electron velocity selectors has permitted narrower energy spreads, the limited electron energy resolution is still somewhat of a problem.

Another difficulty[4] is that in a 1-cm^3 Nier-type ionization chamber, at pressures as low as 10^{-5} Torr, if there is a monolayer of gas on the surface, then there are 10^4–10^5 times more molecules on the walls than in the volume enclosed. The ionization potential of molecules on the wall may be slightly different from that for corresponding free molecules, and thus change the shape of ionization probability curves.

Recent measurements of surface phenomena[4–6] reveal another source of experimental errors. They indicate, for instance, that it is quite difficult to obtain the field-free or at least constant low-field region necessary for accurate measurements of ionization cross sections; and a field in this region, caused by such surface phenomena, can greatly influence the ion collection efficiency as well as broaden the electron energy spread.

Many other sources of systematic errors due to

the apparatus are described by Kieffer and Dunn,[7] and are discussed at the end of this paper insofar as they apply to our experiment.

I. APPARATUS

A. Ion Source

The ion source essentially consists of a molecular beam crossed at 90° by a beam of mono-energetic electrons. The molecular beam is ribbon shaped, and in the collision region has a full-intensity width of 6 mm and a full-intensity thickness of ~1 mm, that is, ±1° with respect to the horizontal plane in Figs. 1 and 2. It is produced by a 0.6×0.02-cm nozzle followed by a 0.6×0.05-cm collimator slit at a distance of 0.7 cm (Fig. 1). Differential pumping between the two sides of the collimator slit is carried out by two water-baffled oil-diffusion pumps having effective pumping speed in the source region of 150 liter-sec^{-1} for pump No. 1 and 300 liter-sec^{-1} for pump No. 2. Pressure measurements indicate a gas flow from the beam of ~10^{16} molecules-sec^{-1} for Ar at 300°K, which agrees well with calculated values, with a nozzle pressure of 0.1 Torr. This pressure in a nozzle slit of these dimensions allows a molecular flow.[8]

The scattering of the beam in the high vacuum region (evacuated by diffusion pump No. 2, Fig. 1) gives rise to a background pressure of ~10^{-6} Torr in our usual operating conditions, as compared to ~10^{-7} Torr without gas. The slit dimensions and the gas flow producing this background allow the

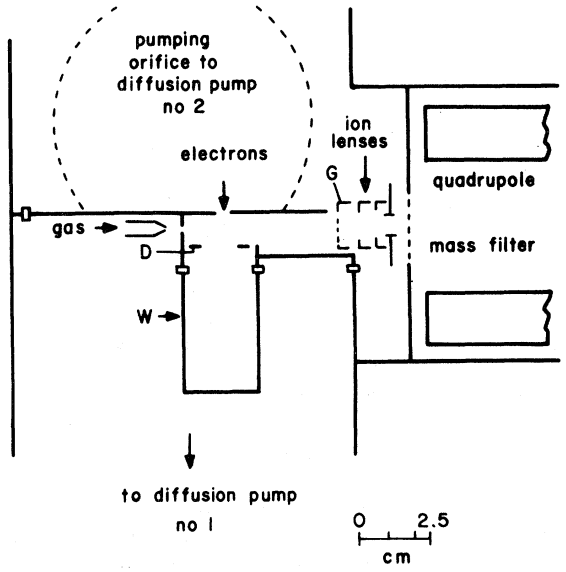

FIG. 1. Side view of the ion source; W: Electron collector well; D: Diaphragm for well W; G: Ion extracting grid.

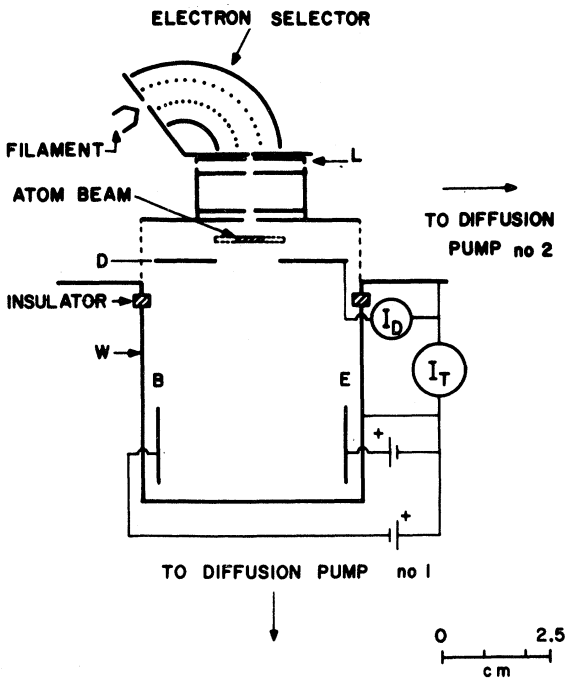

FIG. 2. Front view of the ion source; B and E: Plates maintaining electric field in the well; E: electron collecting plate; L: Electrostatic virtual diaphragm to control the electron current, I_D: Electron current from well-diaphragm D; I_T: Total electron current from D, E, and W. The dashed part of the atom beam shows its full-intensity shape at the center of the collision region. The dotted part is its total width.

calculation of a virtual pressure of ~3×10^{-5} Torr in the beam. It has been verified that the effusion from the nozzle side of the collimator slit to the ionization region is negligible with respect to the background caused by the scattering of the beam.

The electrons from a tungsten filament are selected by a cylindrical electrostatic electron velocity selector[3] having an energy resolution of the order of 0.05 eV at electron currents of up to 10^{-8} A. The selector is entirely made of stainless-steel type 304, except for the entrance slit which is made of soft iron to reduce the magnetic field in the selector region due to the filament current. The grids are made of 100 line per inch etched stainless-steel mesh supplied by Buckbee-Mears Co. The selector is enclosed in a soft-iron box which can be demagnetized[9] to cancel the earth's magnetic field. It also prevents stray electrons from the filament from reaching the ionization region. The selector exit slit is followed by a virtual electrostatic diaphragm L (Fig. 2) that controls the electron current. The electrons are then accelerated to the required energy, and pass through a series of collimators (all at the acceleration potential) that maintain the electron beam

width smaller than $\frac{2}{3}\times$the full-intensity width of the molecular beam. (The electron beam is also ribbon shaped, and its height is parallel to the axis of the molecular beam). The last collimating slit is slightly wider than the preceding one. Its purpose is to reduce the penetration in the ionization region of any surface potential caused by electron bombardment on the edges of the preceding, narrower slit.

The ionization region has been designed to provide maximum ion-collection efficiency for ions produced from molecules having velocities parallel to the axis of the molecular beam; the ions produced from the background due to the scattering of the beam cannot be mass-spectroscopically separated from those of the beam, since they are of the same nature. To reduce their number, as large a pumping speed as possible is needed in the ionization region for a given beam intensity; the surfaces are thus made of mesh wherever possible to allow efficient evacuation of the source.

All surfaces are made of stainless-steel type 304; in particular, those subject to charged particle bombardment are built as far as possible from the beam in order to minimize surface effects such as surface charges.[5,6] This is accomplished in particular by collecting the electrons in a deep well W in which a relatively strong electric field (10 V/cm) is maintained between plates E and B of Fig. 2 to prevent reflected electrons from escaping back into the ionization region, and to collect ions produced in the well. The potential penetration in the beam region due to this field is kept below 10 mV by diaphragm D of Figs. 1 and 2 so that its perturbation of the electron energy distribution is negligible. The well itself is insulated from the other walls of the ionization region so that the total electron current I_T coming through the electron slit can be measured.

The ion extracting field is applied by grid G of Fig. 1 and is adjusted so that the electron energy resolution is not disturbed by more than ~10 mV.

The preferential collection for ions having thermal velocities parallel to the molecular beam, allows a beam-signal over background-signal ratio of up to 30. This is determined by measuring the ion current and the background pressure with the gas coming from the beam, and then dividing by the ion current obtained with the same gas pressure in the source when the gas is introduced by another aperture. This may seem trivial since the virtual pressure in the beam is ~30 times the background pressure. However, the distance travelled by the electrons in the background (~1 cm) is much greater that that in the beam (~1 mm at center of electron beam). The value of 30 obtained makes it unnecessary to modulate the molecular beam.

The virtual diaphragm that is controlled by the electrometer measuring the total electron current on diaphragm D, well W and electron collector plate E (L in Fig. 2), is used to reduce slight electron current variations as a function of electron energy (~3%/eV), and maintains this current constant $\pm$<0.2%/eV at all energies between 10 and 26 eV. The stability as a function of time is a function of that of the zero of the electrometer which can be reset to $\pm$2% of the electron current between each curve. The controlling element L simply reduces the penetration in the selector exit-slit region of the field from the accelerating element of the lens, thereby creating a "potential channel" with a width dependent on the voltage applied to L. The electrons not accepted are reflected backwards and collected either by the selector exit slit or by L. The slit dimensions and spacings are drawn to scale on Fig. 2. The operating voltage of element L is in the vicinity of 0 V with respect to the selector exit slit.

The electron current I_D on diaphragm D can also be separately measured. Its value is approximately 3% of the total electron current I_T, and is virtually independent of electron energy when diaphragm L is operated. We have verified that at all electron energies utilized, the electronic current reflected from the well to the ionization region is less than 1% of the total collected electron current I_T. This has been accomplished by placing an electron collector immediately below (<1 mm) the ionization region entrance slit. This collector covers the full width of the ionization region, and is suitably pierced so that the incident electron beam cannot strike it.

B. Ion Analyzer and Detector

The ions are focused in the entrance (Fig. 1) of a large aperture (2 cm diam), large field radius (2 cm), 1.1-m-long quadrupole mass filter[10] operated at 1 MHz. This instrument is capable of accepting ions having 150-eV axial energy, with up to 1-eV radial energy, and is capable of 100% transmission efficiency (indicated by square-topped mass peaks[10–11]) with a resolution of 1 amu at all masses between 1 and 50.[12] The ions are then focused on and collected by a specially designed and built electron multiplier with ~90% ion detection efficiency.[13] Single-ion pulses are counted so that the ion current measured is independent of the pulse amplitudes. This also allows subsequent digital treatment of the results. A Poisson-type single-ion pulse-height distribution is obtained. This permits discrimination of signal pulses from multiplier noise and constant counting efficiency regardless of multiplier noise fluctuations.[13] The pulse counting system is fast enough so that <1.5% coincidence is obtained at the maximum counting rate for argon.

II. EXPERIMENTAL PROCEDURE

A typical ionization probability (IP) curve consists of 128 points taken at 10-mV intervals, and lasts approximately 10 min. A run consists of up to 20 such curves taken in succession and added automatically on a multichannel analyzer used in the multiscaling mode. Thus all curves are taken into account, no arbitrary relative shifting of individual curves is possible, and no single curve can be rejected. Background due to contaminants of approximately the same e/m as that of the gases being studied has been verified to be negligible.

Since the pressure above pump No. 2 is mostly due to the scattering of the molecular beam, monitoring the pressure would in fact be akin to monitoring the beam intensity. However, ionization gauges drift in time, and furthermore produce ions that interfere with the experiments. The beam intensity is thus not monitored, but the procedure of adding curves to obtain a run cancels out random variations in the curves such as those due to beam variation. Only very slow drifts over several hours could be troublesome. Background pressure measurements at the beginning and at the end of a run indicate that no such drift is measurable.

Electron Energy Distribution

No electron energy analyzer is used because of the need for the electron collecting well. Furthermore, theoretical calculations carried out on our laboratory[14,15] show that the absolute energy distribution width cannot yet be accurately deduced from analyzer data for very narrow energy spreads. An estimate of our energy distribution can however be obtained by double differentiation of our IP curves. Morrison[16] has shown that if the threshold ion current as a function of electron energy follows a simple power law with power close to or equal to 1, as is generally believed,[17–23] the full width at half maximum (FWHM) of the peak in the second derivative of the IP curve gives an upper limit to that of the electron energy spread. In our case, this has the further advantage of yielding the effective energy spread, taking into account any drift between individual curves.

Determination of Appearance Potentials

The ionization threshold energies are compared with that of He, i.e., 24.581 eV as determined spectroscopically. A mixture of He and of the gas being studied is introduced in the system so that no drift can occur between the measurement of the threshold position of both gases, and in case the adsorption of different gases might cause different surface potentials.[7]

III. MATHEMATICAL TREATMENT OF RESULTS

Instead of comparing our data to 1.00,[17–21] 1.127,[22] or 1.5[23] power laws, we fit the summed data for a sum of 15 to 20 curves of a given gas by computer[24] with a simple power law of the form

$$y_i = d + a(c + E_i)^b , \tag{1}$$

where c is the energy above threshold of the first experimental point used in the calculation, E_i is the energy above c of the ith experimental point used, and d is the count rate (background) below threshold. The computer is asked to determine a and b.

To standardize our results, the experimental point to which the value $i = 1$ is assigned is chosen so that a best fit can be obtained with c in the neighborhood of 0.05 eV, to avoid the effects of electron energy distribution near threshold. The best fit is obtained by adjusting the parameters a, b, and c of Eq. (1) to minimize the weighted least-squares expression

$$S = \sum_{i=1}^{n} [(x_i - y_i)/\sigma_i]^2 , \tag{2}$$

where x_i are the experimental values, y_i are the corresponding values calculated according to Eq. (1), n is the number of experimental points used for the calculation and σ_i is the standard deviation at each point x_i; σ_i is taken here to be $x_i^{1/2}$.

No smoothing is carried out either before or after carrying out these calculations when looking for gas structure, as it is evident that smoothing attenuates any sharp feature that may be present in the physical process involved. Adding curves, on the other hand, only attenuates noise.

As pointed out earlier, an upper limit to the combined effects of the electron energy distribution and of the total drift between individual curves is obtained by taking the second derivative of the IP curves. This second derivative being noisy, it must be smoothed a few times by taking for instance $\frac{1}{2}(x_i + x_{i+1})$. This is permissible in this case, because it only increases the upper limit somewhat, and because we are not looking for gas structure in the second derivative. This upper limit may often be well above the true energy distribution, because of the smoothing required. We find, for instance, 0.10-eV FWHM after ten smoothing operations. To determine the energy spread more precisely, curve fitting of the unsmoothed derivative of the IP curve has been attempted, using the least-squares criterion of Eq. (2). The best fitting curve is then differentiated, and the FWHM of the peak thus obtained gives the FWHM of the electron energy distribution plus the drift

from one curve to the other. Functions such as $\mathrm{erf}(x)$, $\tan^{-1}(x)$, and orthogonal polynomials have been used to fit the derivative and give similar values, about 0.07 eV. It is worth noting that ten smoothings of this peak bring its FWHM to 0.10 eV, the same value as that given by the smoothed second derivative of the IP curve. Because of this inaccurate knowledge of the electron energy distribution, no accurate deconvolution[25-26] could be made.

IV. RESULTS

Figures 3 and 4 are the observed IP curves of He and Ar, respectively, with plots of the corresponding derivatives. Note that, on the IP curves, the statistical error is smaller than the size of the data points. As seen in Figs. 3(a) and 4(a), the IP curves of both He and Ar appear to be smooth curves and show no major dissimilarity. The Ar^+ curve in particular shows none of the breaks previously reported,[3,27-39] and its derivative does not appear to have steps other than that at threshold.

The method described above to determine the effective energy resolution gives a value of 0.07 eV for the Ar^+ curve of Fig. 4, indicating that our energy spread is narrow enough to resolve easily the $^2P_{3/2}$ and $^2P_{1/2}$ states.

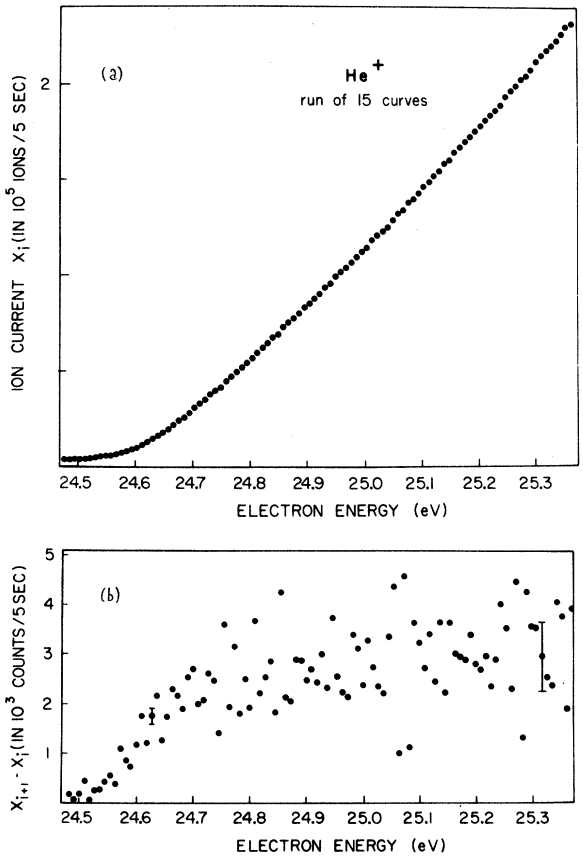

FIG. 3. (a). Ionization curve of He; corrected energy scale (see text). The 5 sec on the vertical axis is the measurement time for one point of a single curve. (b). Derivative $x_{i+1} - x_i$ of the IP curve of He; the error indicated is $\pm (x_{i+1} + x_i)^{1/2}$. Note the enlargement of the vertical scale by a factor of 100 from Fig. 3(a).

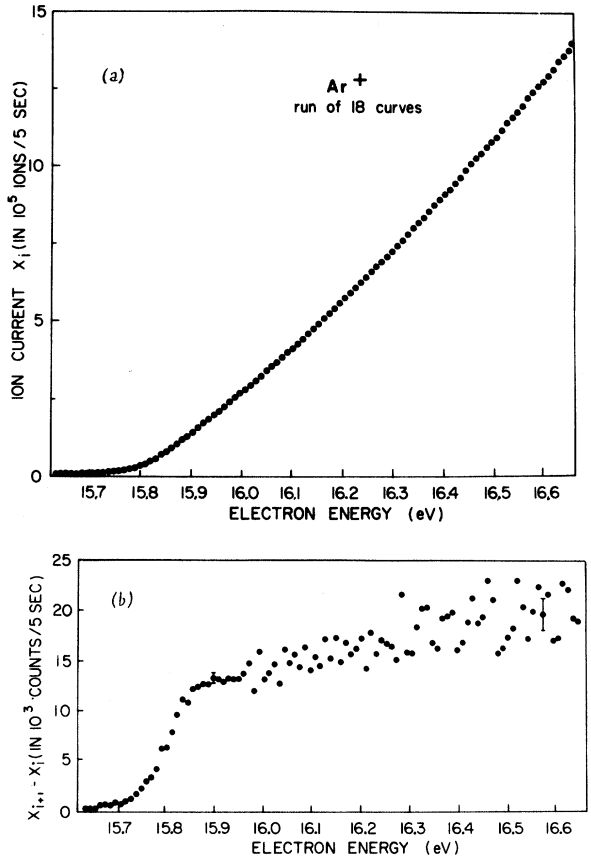

FIG. 4. (a). IP curve of Ar, energy scale calibrated with He^+. The 5 sec on the vertical axis is the measurement time for one point of a single curve. (b). Derivative $x_{i+1} - x_i$ of Ar IP curve. Note the enlargement of the vertical scale by a factor of 100 from Fig. 4(a).

Helium

Figure 5 gives the plot of the relative difference $(x_i - y_i)/x_i$ between the experimental values for He^+ and the best fit obtainable with Eqs. (1) and (2). The computed values for many runs of curves taken months apart are $b = 1.16$, reproducible $\pm 3\%$. Figure 5 shows that Eq. (1) is a very satisfactory expression for the behavior of the ionization cross section of He in the first eV above threshold. To show how good the calculated fit is, Fig. 6 is a plot of $\ln(x_i - d)$ versus $\ln(c + E_i)$. This is a straight line (except for the first point) with slope 1.15.

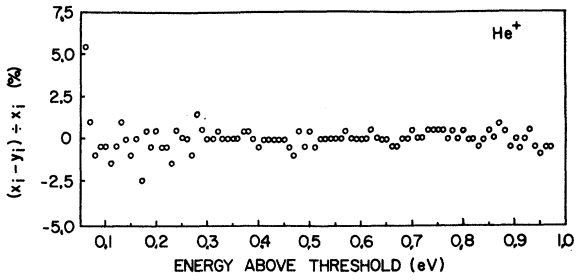

FIG. 5. Relative difference $(x_i - y_i)/x_i$ between the experimental values of He^+ and the best-fitting power law for this curve with power $b = 1.15$; the plot starts ~0.05 eV above threshold (see text) and is shown directly as plotted by the computer.

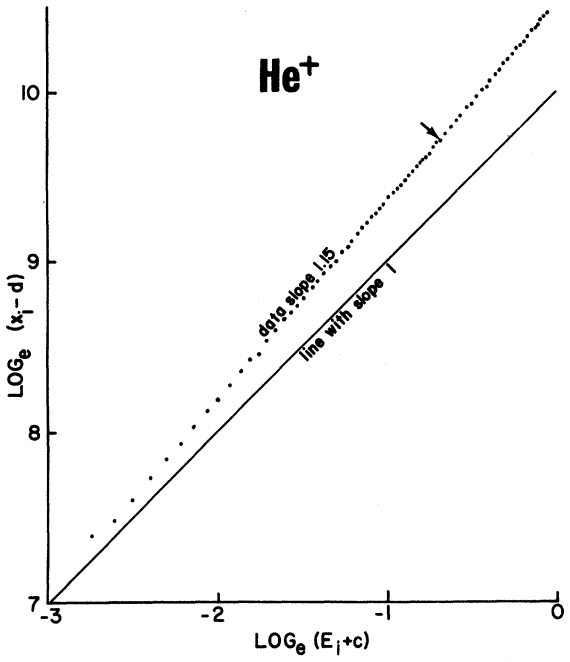

FIG. 6. Plot of $\ln_e (x_i - d)$ versus $\ln_e (E_i + c)$ for the He IP curve of Fig. 3. Above the arrow only every second point is shown for the sake of clarity.

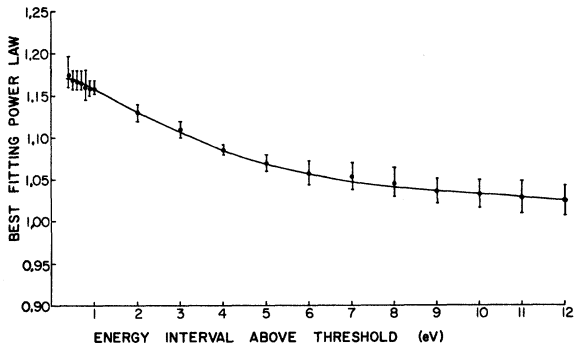

FIG. 7. Plot of best-fitting power law from threshold to indicated energy for helium IP curves measured over 12 eV. The error bars indicate the maximum deviation observed on all our runs.

Many threshold laws have been predicted for single ionization by electron impact[17–23]; reviewed by Rudge.[40] The power law we observe differs only by 3% with the theoretical threshold value 1.127 predicted by Wannier,[22] and with the 1.127 value recently measured by Brion *et al.*[41] and Kirge *et al.*,[42] although they have not shown that this is the best-fitting power for their data. Previous experiments[1,27,31,32,43–50] find a linear law, but the accuracy in the first eV above threshold is generally poor, since the curves are done over many eV. However, our results do not disagree with the latter, since the power decreases with electron energy. If we calculate the best-fitting power law for a helium ionization curve extending for 12 eV above threshold, we find a power of 1.02; reproducible ±2%. To pursue the matter further, we calculated the best-fitting power law from threshold to several energies E between 0.4 and 12 eV using in each calculation data points from threshold to that same energy E. This is shown in Fig. 7. This fit is naturally observed to get worse and worse as the range is extended to several eV, but remains a convenient way of describing the shape of the IP curves as a function of energy. Extrapolation (insofar as it is valid) of this curve toward the lower energies would yield a likely threshold power law with power 1.17.

Argon

We have applied the same techniques to argon. The calculated value of c [Eq. (1)] obtained from the curve fitting allows extrapolation of the threshold energy. This energy is arbitrarily taken to be 24.581 eV for He and is used to calibrate the energy scales in Figs. 3 and 4. The appearance potential of Ar^+, so determined, agrees within 0.03 eV with the spectroscopic value, so we assume it coincides with the $^2P_{3/2}$ level of Ar^+.

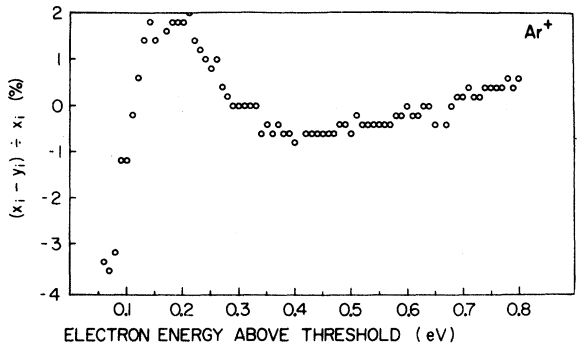

FIG. 8. Relative difference $(x_i - y_i)/x_i$ between our experimental points for Ar^+ and the best-fitting power law with power 1.25; the plot starts ~0.05 eV above threshold (see text) and is shown directly as plotted by the computer.

On the other hand, Fig. 8 shows that the first eV of the Ar IP curve cannot be represented by a simple power law. The peak on Fig. 8 is at approximately 0.2 eV above threshold, very near the expected value for the onset of the $^2P_{1/2}$ state, and is consistently reproducible. Now if a best fit of only the upper part of the IP curve is calculated (above 0.25 eV), a curve such as that of Fig. 9 is obtained, showing that this part closely agrees with a simple power law with power 1.34; reproducible ±4% over many runs. If this function is then extrapolated toward the lower energies, Fig. 10 is obtained.

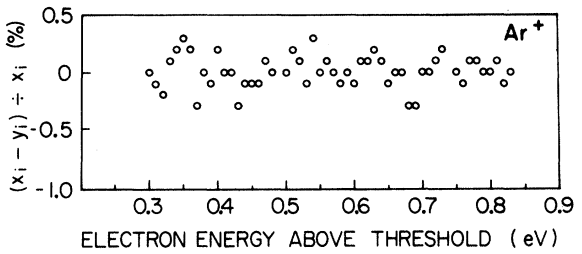

FIG. 9. Comparison of the experimental values of Ar^+ starting 0.25 eV above threshold with the best-fitting power law for these points, having power $b = 1.32$ (shown directly as plotted by the computer).

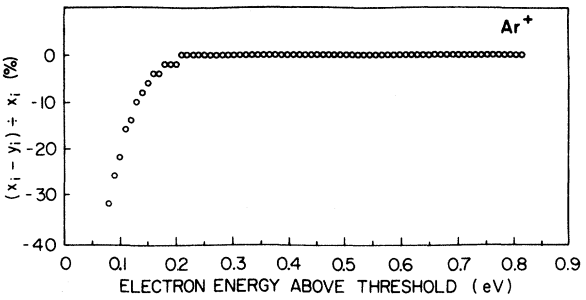

FIG. 10. Comparison of the experimental values of Ar^+ with the extrapolation from 0.25 to 0.05 eV above threshold of the power law of Fig. 9, (shown directly as plotted by the computer).

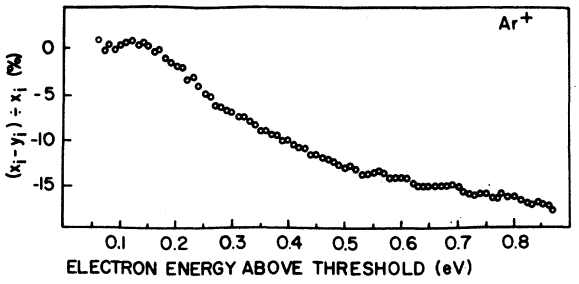

FIG. 11. Comparison of the experimental values of Ar^+ with the extrapolation above 0.25 eV of the best-fitting power law for the points from 0.05 to 0.15 eV above threshold, having power $b = 1.35$.

A fit of the lower part can also be carried out, although the accuracy is much lower because there are only some ten points available. If a simple power law is nonetheless fitted to this part, extrapolated toward the higher energies and compared to the experimental data, a curve such as that of Fig. 11 is obtained. The power is 1.3; reproducible ±15%. This procedure does not exclude the possibility of unresolved autoionized states and structure in this part of the curve.

Our results are compared in Fig. 12 with those of Fox,[27] Marmet and Morrison[43] and Foner and Nall.[28] Their results are typical and may be represented by linear laws with breaks; our curve is almost smooth. We have nonetheless attempted to fit straight lines to our data. For the points between 0.05 and 0.15 eV that should be on a straight line if a linear law with breaks is valid, we calculated S from Eq. (2) for the best-fitting straight line. We find $S = 320$, whereas with our power law, S is 10.5. Similarly, for the points between 0.25 and 0.35 eV, the best-fitting straight line gives $S = 47$, where our power law for these same points yields $S = 26$. We may thus conclude that our Ar^+ data are best represented by two power laws joining at ~0.2 eV above the ionization threshold, where the $^2P_{1/2}$ level should be. This being the case, we

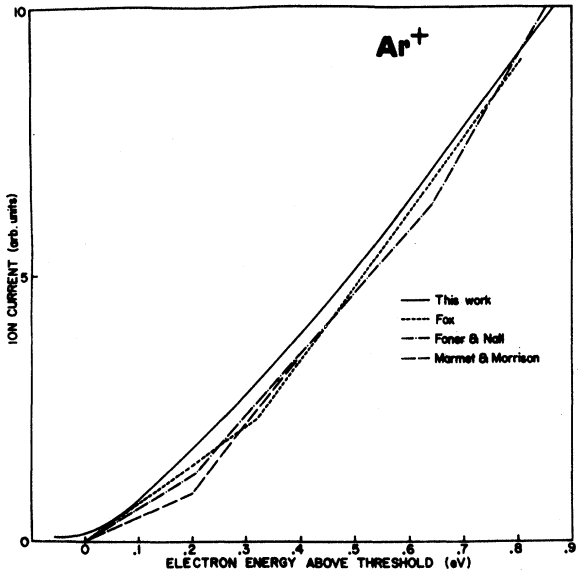

FIG. 12. Comparison of our IP curve for Ar with that of other experimenters: Marmet and Morrison[43], Foner and Nall[28] and Fox.[27] The experimental points are not shown for the sake of clarity. The curves presented are the best-fitting curves given by the respective authors for their data. They have been normalized with ours at the maximum energy given by these authors. That of Marmet and Morrison, however, has been normalized with the two others at its maximum energy, that is 4 eV above threshold.

have not attempted computer fitting of breaks and straight line segments further.[51]

It would also seem, according to Figs. 10 and 11, that the ionization probability function of Ar^+ rises less rapidly above the $^2P_{1/2}$ level than below, and is thus not simply the sum of the cross sections of the $^2P_{3/2}$ and $^2P_{1/2}$ ions. The cross sections of these two states would then be competitive.

V. DISCUSSION OF RESULTS

Reduction of Surface Effects

In the design of our apparatus, the following points have been paid attention to:

(1) The surfaces subject to charged particle bombardment have been either minimized or removed far away from the ionization region. Great care is taken to keep them clean from oil contamination, so that the time needed to produce surface phenomena large enough to influence the ion collection efficiency and thus the shape of the IP curves, is increased to several hundred hours, so that work can be carried out even in a moderate vacuum such as ours. Very slight surface charges can, in fact, alter the ionization curves considerably, since we are dealing with thermal ions having ~0.04 eV energy and since our collection depends to a degree on this thermal velocity. Charges of this order of magnitude varying with time or with electron energy can and do alter the shape of ionization curves considerably.

(2) The use of a molecular beam ensures three times less intermolecular collisions,[52] fewer contacts of atoms and ions with the surfaces, and a lower background pressure.

The minimization of surfaces subject to electron bombardment also minimizes the number of ions produced or exchanged on the surfaces, by comparison with conventional apparatus.

We have verified that the shape (power) of the He^+ curves and the structure observed in Ar^+ are not due to surface phenomena; when the source is clean and has just been introduced into the vacuum system, heating it to ~100°C produces no change at all, either in ion current or in curve shapes. The structure in Ar^+ remains unchanged, and there are no measurable variations in the power of the He^+ curves. On the other hand, after a few hundred hours use, the ion current for given experimental conditions decreases, the shape of the curves changes, and heating the source to ~100°C restores the current and curve shapes to their previous value. This fact we believe to be due to surface charges[5] influencing the ion collection efficiency of the ion optical system. If the structure we observe in Ar^+ were due to these changes, it would then disappear or at least change upon heating the source.[6]

Our results show a very satisfactory reproducibility, day to day and month to month, even after the source has been removed for cleaning. This is certainly not the case with uncontrolled surface phenomena in general. The lack of agreement between different experimenters, who observe different relative cross sections and break energies (as reviewed by Winters *et al.*[34]) could be explained by such surface phenomena since they all use conventional ion sources.

Systematic Errors

We have also investigated the possible sources of systematic errors in our apparatus: (1) Variation of overlap factor between the electron beam and the molecular beam as a function of electron energy; (2) variation of the collection efficiency because of the momentum transfer from the electrons to the thermal molecules near threshold; (3) variation of the mass spectrometer efficiency with electron energy due to different entrance conditions.

(1) The design of the electron optics is intended to minimize changes in the electron beam width. After the virtual diaphragm L, the electrons are immediately accelerated and are collimated by slits in a field-free region. There are thus no lens effects near the exit slit and the electron trajectories are straight lines. Geometrically, the electron beam is at most 4 mm wide at the intersection of the molecular beam, that is, $\frac{2}{3}\times$the full intensity width of the latter. As a test, we have disconnected diaphragm L from the electrometer output, set it at a fixed potential, and carried out some He^+ IP curves. The electron current varies, but is simultaneously recorded. The ion current is then divided at each point by the corresponding electron current, and a best fit of the resulting curve is calculated. In these conditions, we have observed no deviation in the power law greater than the ±3% previously mentioned.

(2) The momentum transfer from the electrons deflects the helium ions at threshold by an average angle of 16° with respect to the neutral beam. However, what is important for the shape of our IP curves is the variation of this angle in a 1 eV interval in the electron energy above threshold. The worst imaginable case occurs when the incident electron and the one ejected from the atom both leave in the same direction, parallel or antiparallel to the incident electron beam, having each half of the excess energy, that is 0.5 eV each at 1 eV above threshold. This would amount to a maximum possible (but unlikely) angle variation of ±6° with respect to the trajectory at threshold. To verify that the collection efficiency of our apparatus is not appreciably angle sensitive, we decreased the ion extracting potential on grid G by half, enough to reduce the ion current by 25%. Reducing the extraction potential should eliminate ions that

make such an angle with the axis as to be at the limit of collection. Once again, no variation in the power law for the first eV of helium was found.

(3) The same kind of test was carried out to show the independence of the power law on the entrance conditions of the mass filter. Unfocusing the ion lenses to reduce the ion current by 30% produced no measurable change in the calculated power.

To conclude, we estimate that the overall error in the power law measured for helium is given by the limits of our reproducibility, that is $\sim \pm 3\%$, since reasonable variations in all pertinent parameters produce no significant variations. For argon, the essential facts are that there are apparently no levels or discontinuities above the $^2P_{1/2}$ level, although there may be many unresolved ones below it.

---

*Work sponsored by the Defense Research Board of Canada, grant No. DRB-9930-13.

[1]R. E. Fox, W. M. Hickham, D. Grove, T. Kjeldaas, Phys. Rev. 84, 859 (1951); Rev. Sci. Instr. 26, 1101 (1955).

[2]C. E. Kuyatt, J. A. Simpson, Rev. Sci. Instr. 38, 103 (1967).

[3]P. Marmet, L. Kerwin, Can. J. Phys. 38, 787 (1960).

[4]P. Marmet, J. D. Morrison, J. Chem. Phys. 36, 1238 (1962).

[5]Y. Petit-Clerc, J. D. Carette, Vacuum 18, 7 (1967).

[6]Y. Petit-Clerc, J. D. Carette, Appl. Phys. Letters 12, 227 (1968).

[7]L. J. Kieffer, G. H. Dunn, Rev. Mod. Phys. 38, 1 (1966).

[8]N. F. Ramsey, Molecular Beams (Clarendon Press, Oxford, England, 1956).

[9]P. Marmet, J. D. Morrison, D. L. Swingler, Rev. Sci. Instr. 33, 239 (1962).

[10]W. Paul, H. P. Reinhard, U. von Zahn, Physik 152, 143 (1958).

[11]H. G. Bennewtiz, R. Wedemeyer, Z. Physik 172, 1 (1963).

[12]P. Marchand, P. Marmet, Can. J. Phys. 42, 1914 (1964).

[13]P. Marchand, C. Paquet, P. Marmet, Rev. Sci. Instr. 37, 1702 (1966).

[14]Y. Delage, J. D. Carette, to be published.

[15]P. Allard, J. D. Carette, to be published.

[16]J. D. Morrison, J. Chem. Phys. 21, 1767 (1953).

[17]S. Geltman, Phys. Rev. 102, 171 (1956).

[18]M. R. H. Rudge, M. J. Seaton, Proc. Phys. Soc. (London) 83, 680 (1964); Proc. Roy. Soc. (London) A283, 262 (1965).

[19]R. K. Peterkop, Proc. Phys. Soc. (London) A77, 1220 (1962).

[20]K. Omidvar, Phys. Rev. Letters 18, 153 (1967).

[21]I. Vinkalns, M. Gailitis, Abstracts of the Contributed Papers of the Fifth International Conference on the Physics of Electronic and Atomic Collisions, 1967 (Nauka, Leningard, 1967), p. 648.

[22]G. H. Wannier, Phys. Rev. 90, 817 (1953).

[23]A. Temkin, Phys. Rev. Letters 16, 835 (1966); and to be published.

[24]We thank the "Centre de traitement de l'Information de l'Université Laval" for the use of an APL/360 console.

[25]J. P. Morrison, J. Chem. Phys. 39, 200 (1963).

[26]T. Moore, Brit. J. Appl. Phys. 1, 237 (1968).

[27]R. E. Fox, J. Chem. Phys. 33, 200 (1960).

[28]S. N. Foner, B. H. Nall, Phys. Rev. 122, 512 (1961).

[29]C. F. Brion, D. C. Frost, C. A. McDowell, J. Chem. Phys. 44, 1034 (1966).

[30]V. Srinivasan, J. A. Rees, Brit. J. Appl. Phys. 10, 59 (1967).

[31]R. K. Asundi, N. V. Kurepa, J. Electron. Control 15, 41 (1963).

[32]R. K. Asundi, Proceedings of the Sixth International Conference on Ionization Phenomena in Gases, Paris, 1963, edited by P. Hubert (S. E. R. M. A., Paris, France, 1964), Vol. I, p. 29.

[33]J. Peresse, F. Tuffin, P. Sinou, Compt. Rend. Acad. Sci. B265, 1214 (1967); B265, 1234 (1967); Phys. Letters 25A, 773 (1967).

[34]R. F. Winters, J. H. Collins, W. L. Courchene, J. Chem. Phys. 45, 1931 (1966).

[35]K. Maeda, F. P. Lossing, in "Proceedings of the Fourteenth Annual Conference on Mass Spectrometry," Dallas 1966, p. 669 (to be published).

[36]P. Marmet, L. Kerwin, E. M. Clarke, Advances in Mass Spectrometry (The McMillan Company, New York, 1963), Vol. II, p. 522.

[37]P. Marmet, J. D. Morrison, J. Chem. Phys. 35, 746 (1961); 36, 1238 (1962).

[38]D. A. Hutchison, Advanc. Mass Spectrometry, 2, 527 (1963).

[39]J. F. Williams, Can. J. Phys. 46, 2339 (1968).

[40]M. R. H. Rudge, Rev. Mod. Phys. 40, 564 (1968).

[41]C. E. Brion, G. E. Thomas, Abstracts of the Contributed Papers of the Fifth International Congress on Physics of Electronic and Atomic Collisions, 1967 (Nauka, Leningrad, 1967), p. 53; Phys. Rev. Letters 20, 241 (1968); Intern. J. Mass Spectr. Ion Phys. 1, 25 (1968).

[42]G. J. Kirge, S. M. Gordon, P. C. Haarhoff, Z. Naturforsch 23a, 1383 (1968).

[43]P. Marmet, J. D. Morrison, J. Chem. Phys. 35, 746 (1961).

[44]C. Blanc, D. Blanc, C. Malesset, J. Phys. Radium 23, 219 (1962).

[45]D. D. Briglia, D. Rapp, Lockheed Missiles and Space Co. technical report No. 6-75-65-2 (unpublished); Phys. Rev. Letters 14, 245 (1965).

[46]R. E. Fox, Advances in Mass Spectrometry (Pergamon

Press, London, 1959), p. 397.

[47]V. H. Dibeler, R. M. Reese, J. Chem. Phys. 31, 282 (1959).

[48]J. D. Morrison, J. Chem. Phys. 21, 1767 (1953).

[49]D. A. Hutchison, Atomic Collision Processes, (North-Holland Publishing Company Amsterdam, 1964) p. 443.

[50]R. K. Curran, J. Chem. Phys. 38, 2974 (1963).

[51]I. I. O. Allison, R. D. Sedgwick, in "Proceedings of the International Mass Spectrometry Conference," Berlin, 1967, p. 20 (to be published).

[52]V. S. Troitskii, Zh. Eksperim. i Teor. Fiz. 41, 389 (1961) [English transl.: Sov. Phys. – JETP 14, 281 (1962)].

PHYSICAL REVIEW VOLUME 180, NUMBER 1 5 APRIL 1969

e-H Resonances in the 2*p* Excitation Channel*

J. William McGowan, J. F. Williams,† and E. K. Curley
Gulf General Atomic Incorporated, San Diego, California 92112
(Received 23 December 1968)

The cross section for the electron-impact excitation of the hydrogen atom to the 2*p* radiative state has been measured from the threshold (at 10.2 eV) to 50 eV. Primary interest is given to the region between the threshold and the $n=4$ level of the hydrogen atom, where several resonances have been identified. An electron-beam resolution of 0.07 eV has been used to study the resonances, while a resolution of 0.18 eV has been used to determine the general behavior of the cross section. Below $n=3$ the ^1S resonances appear to agree with the theoretical predictions, but in the case of the higher angular-momentum ^1D resonance, the agreement between present theory and experiment is poor. Balmer-α excitation is discussed.

I. INTRODUCTION

Theoretical and experimental investigations of the electron-impact excitation of the ground-state hydrogen atom to its first radiative state, the 2*p* state, recently have been reviewed.[1] For electron energies greater than 200 eV, the measured energy dependence of the experimental cross section is best predicted by the Born approximation to the total wave equation, while above about 60 eV, the three-state 1*s*-2*s*-2*p* close-coupling approximation calculations seem to fit the experimental results. There is no calculation which agrees with the experimental values from about 60 eV down to the vicinity of the threshold.

Within several volts of the threshold the three-state close coupling approximation[1–6] again predicts cross-section values approaching to within 40% the values observed experimentally.[7–9] The effect of including higher states in the approximation, i.e., bringing the 3*s*, 3*p*, and 3*d* states into the 1*s*-2*s*-2*p* coupling, is generally to lower the predicted values by about 20%. The effect of adding to the 1*s*-2*s*-2*p* approximation some 20 potential-energy terms which describe electron-electron correlation[10] is to generally reduce the predicted values by another 10%. However, as discussed in this paper, over the first-few electron volts above the threshold, such predicted values are still higher than measured values by about 10%. These discrepancies may well be accounted for by including the full effect of the polarization of the excited states of the target atom.[11]

In the close-coupling approximation, it has been shown, for the $n=2$ and $n=3$ levels, that including coupling to states of the given level results in resonance structure predictions both above and below that level. Recent experimental work[9,12] has confirmed the existence of such resonances in the 2*p* channel just above the $n=2$ threshold.

Recent calculations[13] of the ^1D elastic-scattering resonance below $n=2$ show that for this $l=2$ or *D* state (and perhaps all angular-momentum states $l \geq 2$), the position of the resonance as calculated within the close-coupling approximation depends critically upon the inclusion of higher-lying states of the target atom.

In this paper, attention is given to the 2*p* excitation threshold and the resonance above the $n=2$